State of Charge Estimation of Lithium-Ion Batteries in Electric Drive Vehicles Using Extended Kalman Filtering

Zheng Chen, *Associate Member, IEEE*, Yuhong Fu, and Chunting Chris Mi, *Fellow, IEEE*

***Abstract*—In this paper, a more accurate battery state of charge (SOC) estimation method for electric drive vehicles is developed based on a nonlinear battery model and an extended Kalman filter (EKF) supported by experimental data. A nonlinear battery model is constructed by separating the model into a nonlinear open circuit voltage and a two-order resistance-capacitance model. EKF is used to eliminate the measurement and process noise and remove the need of prior knowledge of initial SOC. A hardware-in-the-loop test bench was built to validate the method. The experimental results show that the proposed method can estimate the battery SOC with high accuracy.**

***Index Terms*—Extended Kalman filter (EKF), hardware-in-the-loop, lithium-ion battery, nonlinear battery model, state of charge (SOC).**

I. Introduction

ELECTRIC drive vehicles (EDVs) have attracted more and more attention because of their capability of displacing fossil fuel consumption and reducing greenhouse gas emissions [1], [2]. Automotive companies have either already produced or about to produce pure electric vehicles (EVs) or plug-in hybrid EVs (PHEVs). The battery system is the most expensive and yet the least reliable component in EDVs today. Vehicle performance is easily affected by battery characteristics, including various factors, such as operating temperature, discharge/charge cycles, charge or discharge rate, and aging of the battery. Accurate calculation of the battery state of charge (SOC) is essential for any battery-powered system that aims at maximizing the battery performance, extending the battery life, and realizing the safe operation of the system, including EDVs [3], [4]. This creates a need for accurate algorithms that can capture the essential application-dependent characteristics of real batteries to estimate/predict battery behavior under various operation conditions.

In theory, the battery SOC can be calculated by the Coulomb counting method through the integration of measured battery current. However, due to measurement errors and noise, aging of the battery, and unknown initial SOC, the calculation of SOC in practice can be cumbersome. Inaccurate SOC will result in reduced performance of the vehicle and potential damage to the battery system. In addition, other battery parameters, such as internal impedance, internal open circuit voltage, polarization constant, etc., are useful information to monitor the battery health conditions, but these parameters cannot be measured directly in real time. Therefore, it is critical to develop algorithms that can estimate the battery SOC and other parameters in real time by utilizing measureable parameters, such as battery current and terminal voltage [5].

Estimation of battery SOC has been extensively studied. In [6], a modeling approach for the scale-up of a lithium-ion polymer battery (LIPB) is reported. A comparison of the experimental discharge curves with the modeling results confirmed that the parameters used to model a small-scale LIPB could be applied to a large-scale LIPB provided the materials and composition of the electrodes as well as the processes for manufacturing the batteries were the same. In [7], a nonlinear model for the lithium battery was built. In [8], the SOC in a battery string is calculated, based on neural networks, which induces a large amount of calculation. In [9], a technique is shown for dynamic battery model identification in automotive applications using linear parameter varying structures. However, aging of the battery and parameter variations are not considered in the studies. For example, measurement noise contributes to significant inaccuracies of SOC and parameter estimations in a battery system.

Advanced methods, such as the Kalman filter, use the measurement observed over time with noise and other inaccuracies and produce values that tend to be closer to the true values over time. It has wide applications in space, military, and other technology developments. The Kalman filter is based on linear dynamic systems discretized in the time domain and is a recursive estimator, which means only the estimated state from the previous time step and the current measurements are needed to compute the estimation for the current state. The extended Kalman filter (EKF) is the nonlinear version of the Kalman filter that linearizes about the current mean and covariance. In [10]–[12], methods based on EKF and predicted the SOC, power fade, capacity fade, and instantaneous available power for lithium-ion battery packs, which are based on different battery models, are proposed. It did not build a precise model with experimental data or give the actual test for the battery of a hybrid EV when it was in operation.

Manuscript received July 5, 2012; revised October 18, 2012; accepted December 10, 2012. Date of publication December 20, 2012; date of current version March 13, 2013. The review of this paper was coordinated by Mr. D. Diallo.

Z. Chen and C. C. Mi are with the Department of Electrical and Computer Engineering, University of Michigan-Dearborn, Dearborn, MI 48128 USA (e-mail: botaoc@gmail.com; chrismi@umich.edu).

Y. Fu was with the Department of Electrical and Computer Engineering, University of Michigan-Dearborn, Dearborn, MI 48128 USA. She is now with General Motors Inc., Warren, MI 48091 USA (e-mail: fuyuhong@gmail.com).

Color versions of one or more of the figures in this paper are available online at http://ieeexplore.ieee.org.

Digital Object Identifier 10.1109/TVT.2012.2235474

Do *et al.* use the Kalman filter to observe the impedance of a Li-ion battery [13]. The key factor for applying EKF to estimate the battery SOC is to build a precise battery model.

In this paper, a battery model and its model parameters are developed based on experimental data, which cover the whole spectrum of battery conditions when the vehicle is in operation. The battery model consists of two parts: 1) an open circuit voltage and 2) a two-order resistance-capacitance (RC) circuit [14], [15]. The open-circuit voltage source is nonlinear, which can describe the relationship between the battery SOC and the open circuit voltage. The two-order RC circuit can reflect the battery dynamic response. The model is validated through experiment data on the test platform. EKF is then used to estimate the battery SOC. It is shown that the proposed algorithm can eliminate the impact of measurement noise and process noise and remove the prior knowledge of the initial SOC.

The rest of this paper is organized as follows. Section II introduces the battery model and derives the state space equations. Section III identifies the battery parameters, simulates the model, and compares the result with the experimental data. Section IV introduces the EKF to identify the battery SOC based on the model built in Section II. Section V introduces the hardware-in-the-loop system to validate the proposed method. The results under two drive cycles, i.e., the urban dynamometer driving schedule (UDDS) and the highway fuel economy driving schedule (HWFET), are shown to prove the feasibility of the proposed algorithm. Finally, Section VI gives the conclusions and summarizes the contributions of this paper.

II. Battery Model

SOC represents the ratio of available capacity and total capacity in the battery. In theory, the battery SOC can be obtained through the Coulomb counting method by integrating the measured battery current

$$s = s_0 - \eta \int_0^t i(\tau) d\tau \tag{1}$$

where $\eta = 1/(3600C)$, s_0 is the initial SOC, and C is the battery capacity in ampere-hours.

The foregoing equation cannot be directly used to calculate the battery SOC due to a few reasons. First, the current integration method relies on the measurement of battery current, which can contain measurement errors and abundant measurement noise. With the current integration approach, the measurement error and noise will accumulate in the SOC calculation during vehicle operations and will affect the accuracy of SOC calculations. Second, the initial SOC may not be known in practice. The goal of this paper is to overcome the foregoing constraints and develop an algorithm that can estimate the battery SOC with acceptable accuracy.

To develop the algorithm for battery SOC estimation, a battery model should be built first. This paper focuses on large-format lithium-ion battery cells for PHEV applications, as shown in Fig. 1. It is a pouch cell lithium-ion battery that

Fig. 1. Lithium-ion porch battery cell used for a PHEV and the study in this paper.

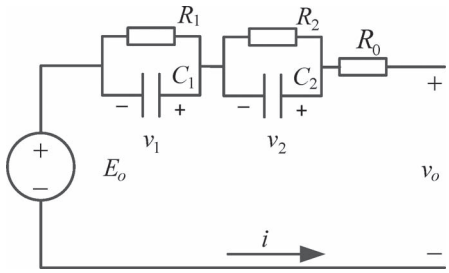

Fig. 2. Equivalent circuit model of the battery.

is used in an original equipment manufacturer (OEM) PHEV. The electrodes and solid electrolyte are usually stacked in layers or laminations and enclosed in a foil envelope. The solid electrolyte permits safer leak-proof cells. The foil construction allows very thin and lightweight cell designs suitable for high power applications. The battery's rated capacity is 20 Ah, the maximum charge voltage is 4.15 V, and the cutoff discharge voltage is 3 V. The maximum continuous discharge current is 100 A. The specific energy is 180 Wh/kg.

The two-order RC circuit, as shown in Fig. 2, can represent the characteristics of a battery as discussed by other scholars [15]–[17]. From Fig. 2, the following equations can be obtained:

$$v_o = E_o + v_1 + v_2 + iR_0 \tag{2}$$

$$i = \frac{v_1}{R_1} + C_1 \frac{dv_1}{dt} = \frac{v_2}{R_2} + C_2 \frac{dv_2}{dt} \tag{3}$$

where v_o is the battery terminal voltage; i is the battery current; and R_0, R_1, C_1, R_2, and C_2 are battery parameters that reflect the battery dynamic response and capacity. v_1 is the voltage drop on capacitor C_1, and v_2 is the voltage drop on capacitor C_2. E_o is the battery internal open circuit voltage.

For further analysis, we choose the voltage drop on the capacitors and the SOC as the state variables. The state space equation can be expressed as

$$\dot{x} = \begin{bmatrix} -\frac{1}{R_1 C_1} & 0 & 0 \\ 0 & -\frac{1}{R_2 C_2} & 0 \\ 0 & 0 & 0 \end{bmatrix} \cdot x + \begin{bmatrix} \frac{1}{C_1} \\ \frac{1}{C_2} \\ -\eta \end{bmatrix} \cdot i \tag{4}$$

where $x = [v_1, \quad v_2, \quad s]^T$, and s is the battery SOC.

We can write the state space function in the standard form

$$\dot{x} = Ax + Bi \tag{5}$$

where

$$A=\begin{bmatrix} -\frac{1}{R_1C_1} & 0 & 0 \\ 0 & -\frac{1}{R_2C_2} & 0 \\ 0 & 0 & 0 \end{bmatrix}, \quad B=\begin{bmatrix} \frac{1}{C_1} \\ \frac{1}{C_2} \\ -\eta \end{bmatrix}.$$

By discretizing the preceding equations, we can get

$$x_k=\begin{bmatrix} -\frac{1}{R_1C_1}\cdot\Delta t+1 & 0 & 0 \\ 0 & -\frac{1}{R_2C_2}\cdot\Delta t+1 & 0 \\ 0 & 0 & 1 \end{bmatrix} \cdot x_{k-1}+\begin{bmatrix} \frac{\Delta t}{C_1} \\ \frac{\Delta t}{C_2} \\ -\eta\cdot\Delta t \end{bmatrix}\cdot i \quad (6)$$

where x_k and x_{k-1} represent the state variables at time steps k and $k-1$, respectively, and Δt denotes the time interval. From (6), the state variables at time step k can be estimated based on the previous step $k-1$.

Under the ideal situation, the foregoing equations can be used to find the battery SOC in two ways.

1) If the initial SOC is known for time step $k-1$, then the above equation directly gives the SOC result at time step k.
2) If the initial SOC is unknown, we can first estimate the state variables v_1 and v_2. Then, we can find the battery open circuit voltage $E_o=v_o-v_1-v_2-iR_0$, where v_o is the measured battery terminal voltage. Since the battery open circuit voltage is directly related to the SOC, we can estimate the battery SOC through a look-up table using the open circuit voltage

$$E_o=f(s) \quad \text{or} \quad s=f^{-1}(E_o) \quad (7)$$

which is determined in advance through testing of the battery under recommended charge and discharge conditions. Therefore, to use the foregoing method, we need to determine the relationship between battery open circuit voltage and SOC and identify the parameters of the battery.

However, the preceding method is difficult to use in practice due to a few reasons. First, the relationship is strongly nonlinear. In particular, many batteries have a flat voltage SOC curve in a large range of SOC. A small measurement error of voltage can cause a large discrepancy of calculated SOC. Second, the measurement error in voltage and current will cause calculation error to accumulate. Hence, additional algorithms need to be introduced to eliminate the impact of measurement noise and the inaccuracies of the battery model.

The next section will discuss how to obtain the battery parameters and determine $E_o=f(s)$ through experiment, and Section IV introduces the EKF to eliminate measurement and process noise as well as considering the sensitivity of SOC estimation due to the inaccuracy of battery parameters.

III. Battery Model Parameter Identification

Based on the model proposed in Section II, each parameter should be determined and validated with data from the experiment.

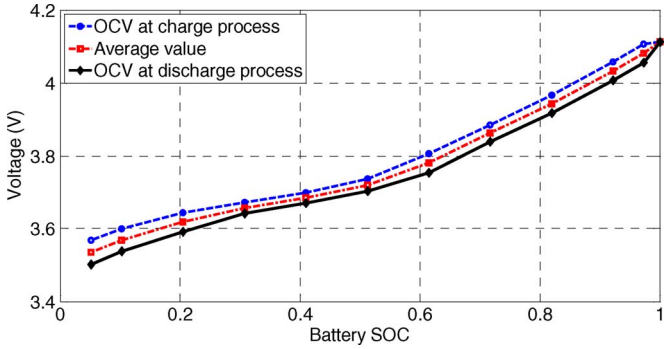

Fig. 3. Relationship between open circuit voltage and SOC.

A. Open Circuit Voltage as a Function of SOC

The battery open circuit voltage has a strong nonlinear relationship with the SOC. We identify the relationship by performing discharge and charge tests of the battery. For charge test, we charge the battery from 0% SOC at factory recommended C/2 rate for 5 min, followed by a rest period of 45 min to allow the cell to return to a charge equilibrium condition before applying the next cycle. The open circuit voltage is then measured. This process is repeated until the battery reaches 100% SOC. For the discharge test, we discharge the battery from 100% SOC at typical 1C rate for 5 min, followed by a rest period of 45 min to allow the cell to return to a charge equilibrium condition before applying the next cycle. The open circuit voltage is then measured. This process is repeated until the battery reaches 0% SOC. Fig. 3 shows the measured open circuit voltage at different SOCs during charge and discharge processes. It can be found that the open circuit voltage during charging is different from that during discharging. Obviously, the open circuit voltage during the charging process is higher than that during the discharging process, and there exists a hysteresis between the two voltage curves. In this paper, we will neglect the hysteresis and adopt their average value to build the model.

Through curve fitting, we found that the open circuit voltage of the battery as a function of SOC can be represented as a seventh-order polynomial equation

$$v_o=a_1s^7+a_2s^6+a_3s^5+a_4s^4+a_5s^3+a_6s^2+a_7s+a_8 =f_1(s) \quad (8)$$

where a_1 to a_8 are the coefficients obtained by the least square method: $a_1=8.4073$, $a_2=-19.892$, $a_3=11.497$, $a_4=4.161$, $a_5=-4.5533$, $a_6=0.34365$, $a_7=0.64685$, and $a_8=3.5016$.

B. RC Circuit Parameters

We identify the RC circuit parameters of matrixes A and B in (5) by performing pulsed charge and pulsed discharge tests of the battery, as shown in Fig. 4. Each cycle consists of a pulsed charge and a pulsed discharge, a constant current discharge, followed by a 45-min rest period to allow the cell to return to a charge equilibrium condition before applying the next cycle.

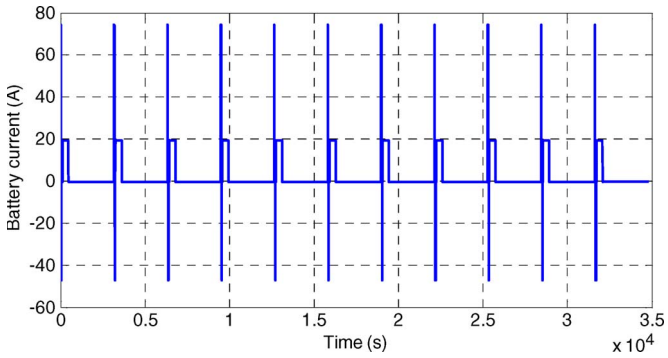

Fig. 4. Battery current profile for circuit parameter identification.

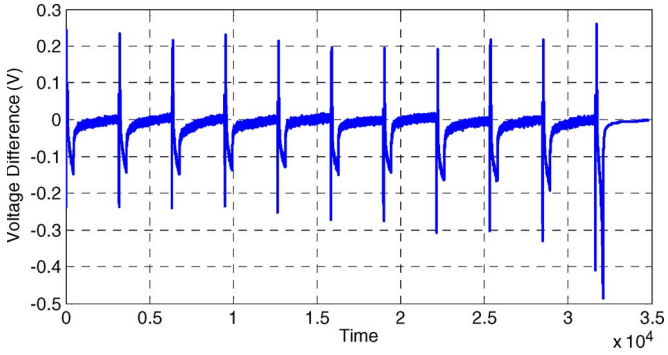

Fig. 5. Differences between battery terminal voltage and open circuit voltage.

This way, the battery's dynamic and steady-state performance can be captured sufficiently. The pulsed charge and pulsed discharge both last 10 s, and the constant current discharge process sustains 5 min. The pulsed charge and discharge current can reach 48 and 75 A, respectively. The difference between battery voltage and open circuit voltage with the same SOC is shown in Fig. 5.

The least-square estimation method is applied to estimate the system parameters through finding the minimum sum of squared error between the system output and the model output.

As shown in (2)–(4), we define $v_d = v_o - E_o$, where v_d is the voltage difference between battery terminal voltage v_o and the open circuit voltage E_o, i.e.,

$$v_d = v_1 + v_2 + iR_0. \tag{9}$$

Based on (2)–(4), and (9), we can get system's transfer function

$$\begin{aligned} V_d &= \left(\frac{R_1}{1+R_1C_1S} + \frac{R_2}{1+R_2C_2S} + R_0\right)\cdot I \\ &= \left(\frac{\left(\frac{1}{C_1}+\frac{1}{C_2}\right)S + \frac{R_1+R_2}{R_1R_2C_1C_2}}{S^2 + \left(\frac{1}{R_1C_1}+\frac{1}{R_2C_2}\right)S + \frac{1}{R_1R_2C_1C_2}} + R_0\right)\cdot I. \end{aligned} \tag{10}$$

The foregoing transfer function can be written into the differential form

$$\begin{aligned} &V_d(n+2) + a_1V_d(n+1) + a_2V_d(n) \\ &\qquad = b_0I(n+2) + b_1I(n+1) + b_2I(n) \end{aligned} \tag{11}$$

where n denotes the time step; a_1, a_2, b_0, b_1, and b_2 are equation coefficients to be estimated; and $a_1 = 1/(R_1C_1) + 1/(R_2C_2)$, $a_2 = 1/(R_1R_2C_1C_2)$, $b_0 = R_0$, $b_1 = (R_0+R_1)/(R_1C_1) + (R_0+R_2)/(R_2C_2)$, and $b_2 = (R_1+R_2+R_0)/(R_1R_2C_1C_2)$.

Suppose we have k sets of data, as shown in matrix form in (12), shown at the bottom of the page.

Define P_d, Y_d, and H_d shown at the bottom of the page, where $[]^T$ denotes the transposition of a matrix.

Therefore, (12) can be changed into

$$Y_d = H_d \cdot P_d. \tag{13}$$

The least square method can be applied to estimate the parameters based on the following calculation:

$$P_d = \left(H_d^T \cdot H_d\right)^{-1} \cdot H_d^T \cdot Y_d \tag{14}$$

$$\begin{bmatrix} V_d(n+2) \\ V_d(n+3) \\ \vdots \\ V_d(n+k+1) \end{bmatrix} = \begin{bmatrix} -V_d(n+1) & -V_d(n) & I(n+2) & I(n+1) & I(n) \\ -V_d(n+2) & -V_d(n+1) & I(n+3) & I(n+2) & I(n+1) \\ \vdots & \vdots & \vdots & \vdots & \vdots \\ -V_d(n+k) & -V_d(n+k-1) & I(n+k+1) & I(n+k) & I(n+k-1) \end{bmatrix} \cdot \begin{bmatrix} a_1 \\ a_2 \\ b_0 \\ b_1 \\ b_2 \end{bmatrix} \tag{12}$$

$$P_d = [\,a_1 \quad a_2 \quad b_0 \quad b_1 \quad b_2\,]^T$$

$$Y_d = [\,V_d(n+2) \quad V_d(n+3) \quad \cdots \quad V_d(n+k+1)\,]^T$$

$$H_d = \begin{bmatrix} -V_d(n+1) & -V_d(n) & I(n+2) & I(n+1) & I(n) \\ -V_d(n+2) & -V_d(n+1) & I(n+3) & I(n+2) & I(n+1) \\ \vdots & \vdots & \vdots & \vdots & \vdots \\ -V_d(n+k) & -V_d(n+k-1) & I(n+k+1) & I(n+k) & I(n+k-1) \end{bmatrix}$$

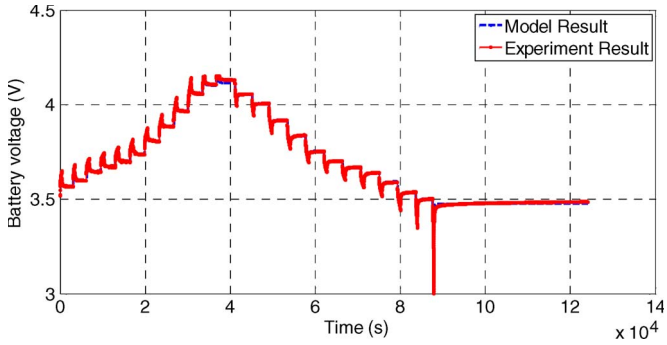

Fig. 6. Model output and experiment result under 10-A charge and discharge.

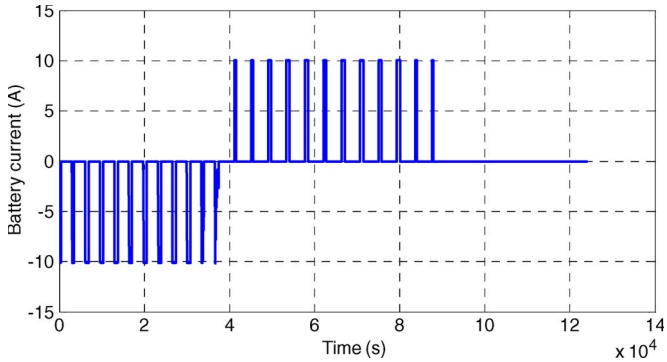

Fig. 7. Battery current.

where $(\ )^{-1}$ denotes the inverse of a matrix. As such, the battery parameters can be obtained based on the estimated P_d accordingly.

Based on the least square identification method and the current shown in Fig. 4 as the input and the voltage difference in Fig. 5 as the output, the parameters A and B can be identified as follows:

$$A = \begin{bmatrix} -0.014 & 0 & 0 \\ 0 & -1.135 & 0 \\ 0 & 0 & 0 \end{bmatrix}$$

$$B = \begin{bmatrix} 5.8442e-5 & 2.2698e-3 & -1.3889e-5 \end{bmatrix}^T.$$

To confirm the validity of the model, various charge and discharge cycles were conducted. The model needs the battery SOC to calculate the battery open circuit voltage through (8). During this time, the battery SOC is obtained by the Coulomb counting method. Fig. 6 shows the measured battery voltage and model output, whose input, i.e., battery current, is shown in Fig. 7. It can be seen that the model could simulate the battery's steady-state and dynamic responses.

Fig. 8 shows the comparison of measured and predicted battery voltage under 20-A constant current discharge. It can be seen that the battery voltage predicted based on the model follows the measurement except when the SOC is very low. In EDVs, the battery operation range is usually from 30% to 100% SOC. Hence, the accuracy of the model is acceptable for SOC estimation in EDVs.

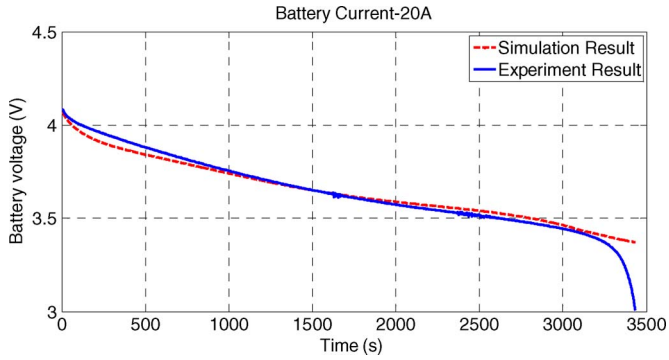

Fig. 8. Model output and experiment result under 20-A constant current discharge.

IV. Extended Kalman Filter

The battery SOC obtained based on the Coulomb counting method relies on the measurement of battery current. Unfortunately, current measurement contains measurement errors and abundant measurement noise. The current measurement error and noise will accumulate in the SOC calculation during vehicle operations and will affect battery management and vehicle energy management. In this section, we introduce EKF to mitigate the influence of measurement error in the SOC estimations. At the mean time, reliance on the initial SOC can be lightened.

The Kalman filter is an established technology for dynamic system state estimation, which has been commonly used in many fields, such as target tracking, global positioning, navigation, and communication. The Kalman filter obtains the minimum mean-square state error estimate. The EKF is the nonlinear version of the Kalman filter that linearizes the current mean and covariance [18]. The nonlinearity of the systems' dynamics is approximated by a linearized version of the nonlinear system model around the last state estimate.

For a nonlinear state-space model

$$\begin{cases} x(t+1) = f\left(x(t), u(t)\right) + w(t) \\ y(t) = h\left(x(t)\right) + v(t) \end{cases} \tag{15}$$

where $u(t)$ is the system input, $x(t)$ is the system state, $y(t)$ is the output, and $f(x(t), u(t))$ and $h(x(t))$ are the nonlinear system functions. The random variables $w(t)$ and $v(t)$ represent the process and measurement noise, respectively, i.e.,

$$\begin{cases} w(t) \sim N\left(0, Q(t)\right) \\ v(t) \sim N\left(0, R(t)\right). \end{cases} \tag{16}$$

Here, we assumed $w(t)$ and $v(t)$ to be independent, white, and with normal probability distributions [18]. $Q(t)$ and $R(t)$ are the process noise covariance and measurement noise covariance that may change with time.

A. Definition

The matrices A_{k-1} and C_k are defined as follows:

$$A_{k-1} = \left.\frac{\partial f(x_{k-1}, u_{k-1})}{\partial x_{k-1}}\right|_{x_{k-1}=\hat{x}_{k-1}} \tag{17}$$

$$C_k = \left.\frac{\partial h(x_k, u_k)}{\partial x_k}\right|_{x_k=\hat{x}_k^-} \tag{18}$$

where A_{k-1} is the Jacobian matrix of partial derivatives of f with respect to x_{k-1} and u_{k-1}, and C_k is the Jacobian matrix of partial derivatives of h with respect to x_k and u_k [18].

If a variable is computed before any system measurements are made, it is denoted by superscript "$^-$", and "$\hat{}$" is *a posteriori* state estimate. For example, $\hat{x}_k^-$ is defined as *a priori* state estimate at step k given the process prior to step k, and $\hat{x}_{k-1}$ is *a posteriori* state estimate at step $k-1$. A prior estimate error e_k^- and a poster estimate error e_k are defined as

$$\begin{cases} e_k^- = x_k - \hat{x}_k^- \\ e_k = x_k - \hat{x}_k. \end{cases} \tag{19}$$

A prior estimate error covariance P_k^- and *a posteriori* estimate error covariance P_k are defined [18] as follows:

$$\begin{cases} P_k^- = E\left[e_k^- e_k^{-T}\right] \\ P_k = E\left[e_k e_k^T\right] \end{cases} \tag{20}$$

where E denotes the covariance.

B. Computation

The EKF estimates the states and process through using a series feedback control, which can be separated into two parts: time update and measurement update. The time update is responsible for predicting forward the current state and error covariance estimates to obtain prior estimates for the next step observation, whereas the measurement update is for the feedback, which bases on the new measurement to obtain an improved *posteriori* estimate.

Therefore, the calculation consists of five steps, i.e., state estimate time update, error covariance time update, Kalman gain matrix calculation, state estimate measurement update, and error covariance measurement update, which are carried out in sequence in (21), shown at the bottom of the page, where L_k is the Kalman gain matrix. I denotes the unity matrix, and P_k is the estimation error covariance at time step k. The whole recursive calculation can be depicted in Fig. 9.

From (21) and Fig. 9, the filter output is calculated only based on the former state and the current system output. Therefore, it does not depend on historical data, which will increase the storage and calculation. Essentially, the EKF makes an optimum tradeoff between sensor reading and model output to achieve the best possible state estimate. In addition, the EKF is not sensitive with the initial value, and it can update or modify the output through the measurement and the model output. Based on this feature, it can be used in the battery SOC identification without knowing the initial SOC, compared with the Coulomb counting method, which needs to determine the initial SOC in advance.

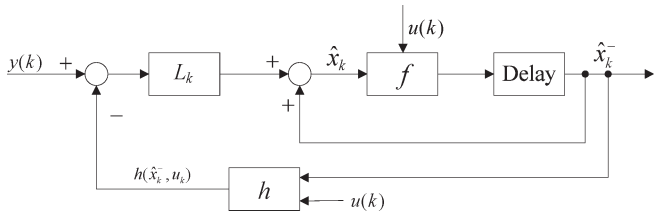

Fig. 9. Blok diagram of EKF calculation.

C. Realization of SOC Estimation

The main computation to realize the proposed SOC estimation algorithm at each measurement interval k is summarized as follows:

State estimate time update

$$\hat{x}_k^- = A_{k-1}\hat{x}_{k-1} + Bi_{k-1} \tag{22}$$

where A_{k-1} and B are the system state matrixes that are constants, as shown in (6), and i is the battery current.

The error covariance time P_k^- update

$$P_k^- = A_{k-1}P_{k-1}A_{k-1}^T + Q(t) = A_{k-1}P_{k-1}A_{k-1}^T + Q \tag{23}$$

where $Q(t)$ is assumed unchanged, and $Q(t) = Q$. We define

$$\begin{aligned} y = v_o &= v_1 + v_2 + E_o + iR_0 \\ &= v_1 + v_2 + f(s) + iR_0 \end{aligned} \tag{24}$$

and therefore, $C_k = [1 \quad 1 \quad \partial f(\hat{s}_k^-)/\partial \hat{s}_k^-]$, and the Kalman gain matrix L_k calculation is

$$L_k = P_k^- C_k^T \left[C_k P_k^- C_k^T + R(t)\right]^{-1} \tag{25}$$

where $R(t)$ is the battery voltage error covariance and dependent on voltage sensor precision. We assume $R(t)$ is a constant R, i.e.,

$$\begin{aligned} \frac{\partial f\left(\hat{s}_k^-\right)}{\partial \hat{s}_k^-} = {} & 7a_1\left(\hat{s}_k^-\right)^6 + 6a_2\left(\hat{s}_k^-\right)^5 + 5a_3\left(\hat{s}_k^-\right)^4 \\ & + 4a_4\left(\hat{s}_k^-\right)^3 + 3a_5\left(\hat{s}_k^-\right)^2 + 2a_6\left(\hat{s}_k^-\right) + a_7 \end{aligned} \tag{26}$$

where $\hat{s}_k^-$ and $\hat{s}_k$ are SOC *priori* and *posteriori* estimates at step k, respectively.

$$\begin{cases} \hat{x}_k^- = f(\hat{x}_{k-1}, u_{k-1}), & \text{State estimate time update} \\ P_k^- = A_{k-1}P_{k-1}A_{k-1}^T + Q(t), & \text{Error covariance time update} \\ L_k = P_k^- C_k^T \left[C_k P_k^- C_k^T + R(t)\right]^{-1}, & \text{Kalman gain matrix} \\ \hat{x}_k = \hat{x}_k^- + L_k\left[y_k - h\left(\hat{x}_k^-, u_k\right)\right], & \text{State estimate measurement update} \\ P_k = (I - L_k C_k)P_k^-, & \text{Error covariance measurement update} \end{cases} \tag{21}$$

TABLE I
MAIN VEHICLE PARAMETERS

Vehicle type	parallel plug-in HEV
Vehicle Mass	2015kg
Engine power	41kW
Motor Power	75kW
Battery	300V, 40Ah

System estimate measurement update:

$$\hat{x}_k = \hat{x}_k^- + L_k\left[y_k - C_k\hat{x}_k^- - iR_0\right]$$
$$= \hat{x}_k^- + L_k\Big[y_k - \hat{v}_{1,k}^- - \hat{v}_{2,k}^- - iR_0 - \frac{\partial f(\hat{s}_k^-)}{\partial \hat{s}_k^-}$$
$$\left(a_1(\hat{s}_k^-)^7 + a_2(\hat{s}_k^-)^6 + a_3(\hat{s}_k^-)^5\right.$$
$$+ a_4(\hat{s}_k^-)^4 + a_5(\hat{s}_k^-)^3 + a_6(\hat{s}_k^-)^2$$
$$\left. + a_7\hat{s}_k^- + a_8\right)\Big]. \quad (27)$$

The error covariance update calculation is realized based on (21) and the calculated parameters P_k^-, C_k, and L_k. Based on the foregoing calculation, the battery SOC can be estimated. The method provides the following advantages.

1) Through EKF, measurement and process noise are removed.
2) Although the method was based on known battery parameters, the actual prediction is no longer sensitive to parameter accuracy due to the self-tuning of the algorithm.
3) The initial SOC need not to be known. The algorithm will automatically converge to the true SOC after a period of time, usually within 2 min, which should be adequate for EV operations.

V. HARDWARE-IN-THE-LOOP VALIDATION

To verify the feasibility of the proposed SOC estimation algorithm, it is essential to validate it through experiments. A hardware-in-the-loop test provides an easy and fast approach to test the proposed algorithm and simulate the actual vehicle operation under different drive cycles. In the system, an EDV is simulated with the main vehicle parameters shown in Table I.

According to the foregoing data, a scaled-down cell-level hardware-in-the-loop system is developed to test the battery under different drive cycles, as shown in Fig. 10. The system includes a charge subsystem, a discharge subsystem, and a data-acquisition system. All the subsystems are connected with a real-time controller DS1104, which is a product of dSPACE, that can determine the charge/discharge strategy; acquire current, voltage, and temperature through A/D ports; and control the charge subsystem and discharge subsystem. It can also calculate the battery SOC with different methods and simulate the vehicle model, which includes engine, motor, and related energy management strategy. A programmable power supply is used as charger, which can supply up to 600-A current and 10-V

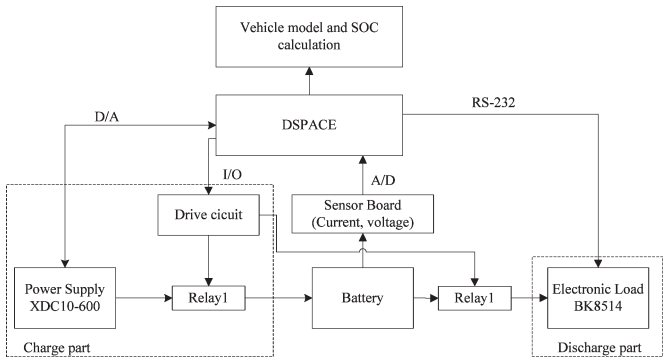

Fig. 10. Test bench system configuration.

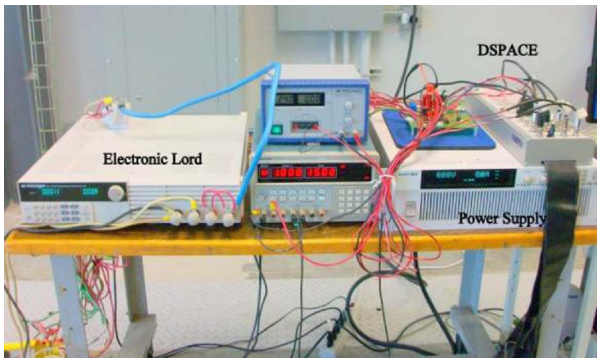

Fig. 11. Test bench.

voltage. A programmable electronic load that could sink up to 120-A current is utilized as the discharge load. The current sensor is a standard automotive sensor, whose sensitivity is within 1%. The test bench is shown in Fig. 11. A battery cell is tested, which has a nominal capacity of 20 Ah, with maximum voltage of 4.15 V and cutoff voltage of 3 V.

The vehicle is simulated under UDDS and HWFET drive cycles based on charge-depleting control strategy of a PHEV [19]. The UDDS drive cycle represents city driving conditions. It is used for light duty vehicle testing. The HWFET drive cycle represents highway driving conditions under 60 mi/h. The vehicle's battery pack consists of 82 battery cells, which is constructed with two cells in parallel as a group and 41 groups in series. Neglecting the difference of the two parallel cells, the current flowing through the cell is half of the battery pack current. All the experiments are carried out at room temperature. The current command along with the actual battery cell current profile based on UDDS and HWFET is shown in Figs. 12 and 13, respectively. It can be seen that the measured current profiles are almost the same as the current commands. Thus, it proves the feasibility of the system.

Based on the model and the current, which is integrated to estimate the SOC with the predetermined initial value, the battery voltage can be calculated to compare with the actual measurement. Fig. 14 shows the model output and the actual battery voltage under UDDS drive cycle, and the difference between them is shown in Fig. 15, in which the maximum difference is limited within 0.06 V. Therefore, the built model is effective to simulate the battery's performance.

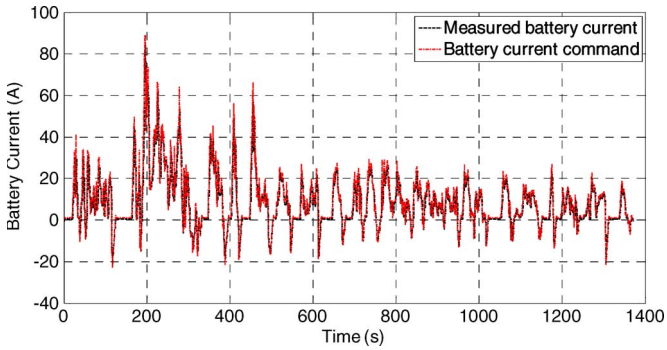

Fig. 12. Battery current based on UDDS drive cycle test.

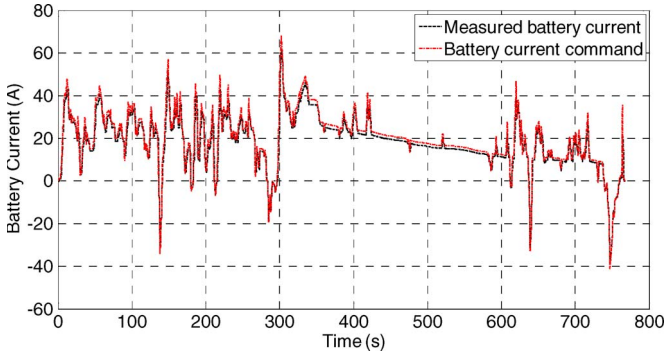

Fig. 13. Battery current based on HWFET drive cycle test.

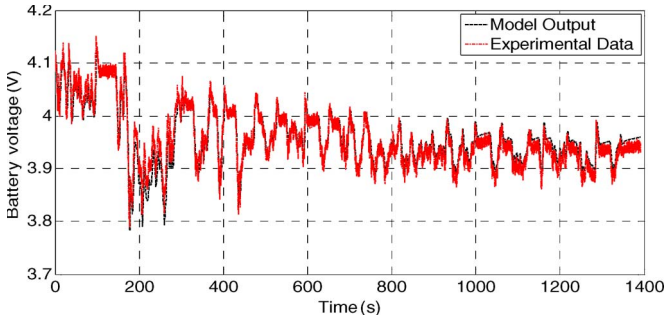

Fig. 14. Battery voltage comparison.

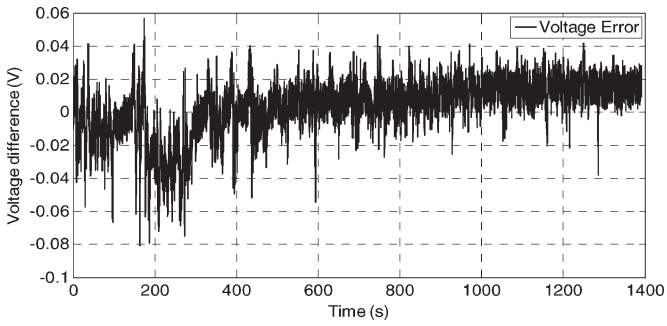

Fig. 15. Voltage difference between actual voltage sensor and model output.

A. SOC Estimation With Known Initial SOC

An experiment is carried out under the HWFET drive cycle. The estimated battery SOC based on the proposed algorithm, and the Coulomb counting method is shown in Fig. 16. The battery is fully charged before conducting the experiment, so the initial SOC is 100%. In (23) and (25), R is set to 1000, and Q is set to

$$Q = \begin{bmatrix} 0.1 & 0 & 0 \\ 0 & 0.1 & 0 \\ 0 & 0 & 0.01 \end{bmatrix}.$$

The initial state error covariance P, after some tuning, is chosen as

$$P = \begin{bmatrix} 0.1 & 0 & 0 \\ 0 & 0.1 & 0 \\ 0 & 0 & 0.01 \end{bmatrix}.$$

In Fig. 16, the maximum battery SOC difference can reach up to 2%. After finishing the experiment, the battery is fully discharged on the calibration platform. Based on its specification, the battery's voltage drops to 3 V when the SOC reaches 0. The ending SOC after the HWFET drive cycle test based on the Coulomb counting method and the EKF method as well as the calibrated value are listed in Table II, which also includes the test results under the UDDS drive cycle.

From Table II, we can see that the ending SOC based on the Coulomb counting method and the EFK method under HWFET drive cycle is 79.60% and 77.80%, respectively. The calibrated value is 74.56%. It can be concluded that the result based on the EKF method under the HWFET drive cycle is closer to the actual SOC than that based on the Coulomb counting method. The experiment results under the UDDS drive cycle also show the consistency. Therefore, the proposed method is more accurate than the Coulomb counting method.

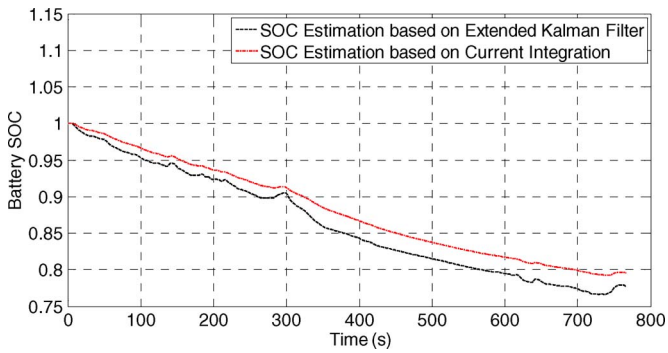

Fig. 16. Battery SOC estimation under HWFET drive cycle.

TABLE II
ENDING SOC COMPARISON UNDER HWFET AND UDDS DRIVE CYCLE

Drive cycle	Coulomb counting	EKF method	Calibrated value
HWFET	79.60%	77.80%	74.56%
UDDS	83.57%	81.90%	78.28%

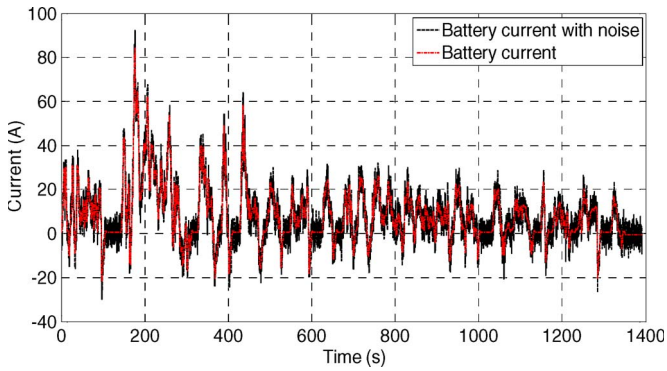

Fig. 17. Comparison of battery current when noises are added to the measurement.

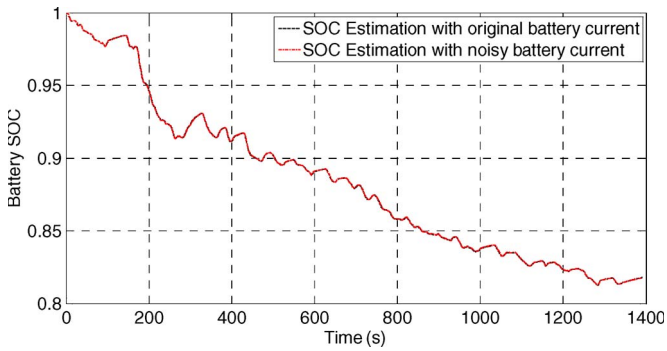

Fig. 18. Battery SOC comparison based on the original battery current and with noise added.

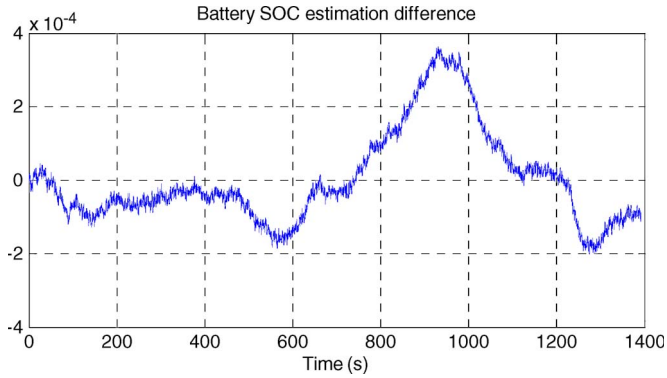

Fig. 19. Battery SOC estimation difference.

B. SOC Estimation With Added Current Noise

To verify the system's performance of removing noise, a random white noise, whose variance equals 10 A^2, is added into the measured current signal. The comparison of current before and after adding the noise under the UDDS drive cycle is shown in Fig. 17, in which the amplitude of the current noise can reach up to 5 A. Fig. 18 shows the estimated SOC using the EKF method based on the original measured current and the noisy current. We can see that the SOC is almost the same. Fig. 19 presents their difference, whose maximum value is limited within 0.04%. It can be concluded that the proposed method is immune to measurement and process noise.

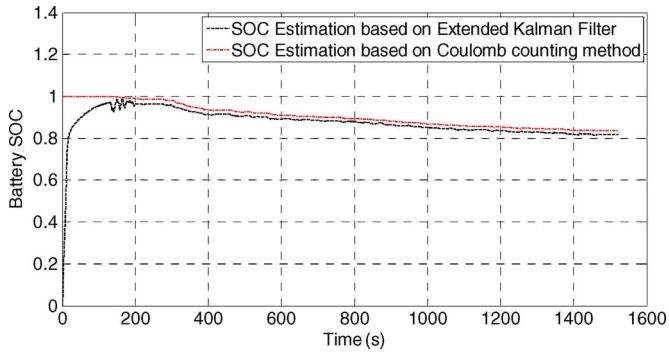

Fig. 20. SOC estimation based on EKF without knowing the initial SOC.

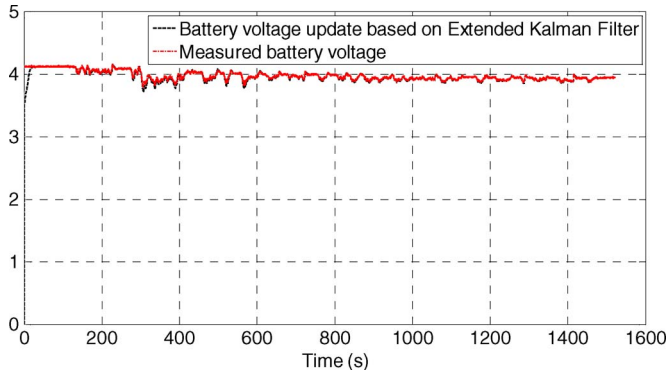

Fig. 21. Comparison of predicted and measured battery voltage.

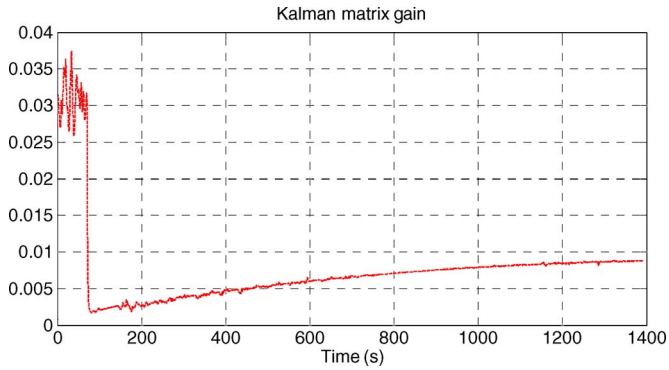

Fig. 22. Kalman matrix gain.

C. SOC Estimation With Unknown Initial SOC

Based on the proposed method with unknown initial SOC, the battery SOC is estimated under the UDDS drive cycle, as shown in Fig. 20, which also presents the SOC estimated through the Coulomb counting method with known initial SOC. The actual initial battery SOC is 100%. To validate the EKF method's feasibility, we assume that the initial SOC is 0 for the proposed method and its initial covariance is 0.1. After 200 s, the covariance of SOC is assumed to be 0.01. The results show that the estimated battery SOC can converge from 0 to the actual value within 100 s.

Fig. 21 shows the model output and the measured battery voltage. The model output converges to the measured value within 50 s. The Kalman matrix gain is shown in Fig. 22, in

TABLE III
MODIFIED BATTERY PARAMETERS TO VALIDATE SENSITIVITY OF THE PROPOSED ALGORITHM

Parameters	True Value	Parameters Group 1	Parameters Group 2	Parameters Group 3
R_0	0.0013Ω	0.0020Ω	0.0008Ω	0.0008Ω
R_1	0.0042Ω	0.0060Ω	0.0030Ω	0.0060Ω
C_1	17111F	20000F	13000F	20000F
R_2	0.0024Ω	0.0030Ω	0.0010Ω	0.0010Ω
C_2	440.57F	650.00F	200.00F	200.00F

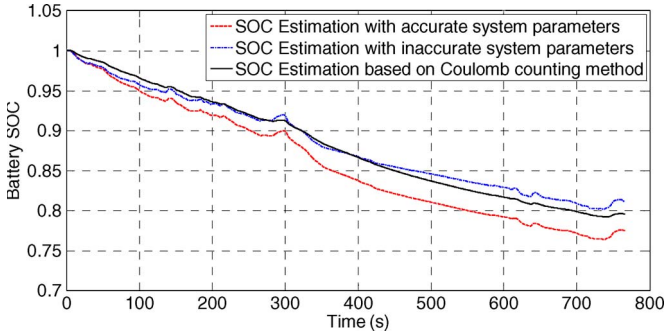

Fig. 23. Battery SOC estimated based on EKF with group 1 parameters.

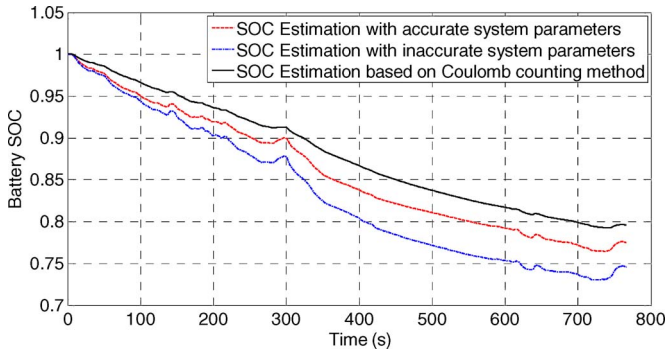

Fig. 24. Battery SOC estimated based on EKF with group 2 parameters.

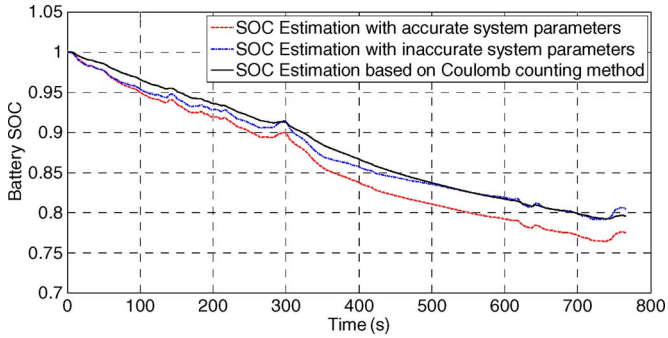

Fig. 25. Battery SOC estimated based on EKF with group 3 parameters.

which we can find that it reaches 0.03 to compensate the SOC difference in the beginning. After the SOC converges to the actual value, the Kalman gain decreases to 0.002 and tends to be stable at 0.008.

D. SOC Estimation With Inaccurate Battery Parameters

With the proposed algorithm, the reliance on battery parameters is still sensitive, but the sensitivity is greatly reduced. To validate this, we modify the battery parameters, as shown in Table III.

From Table III, in group 1, all the parameters increase on average by 50%, and on the contrary, in group 2, all the parameters decrease on average by 50%. In group 3, two parameters R_1 and C_1 increase while the other three parameters R_0, R_2, and C_2 decrease. In group 3, R_1 and C_1 change from 0.0042 Ω, 17111F to 0.0060 Ω, 20 000F; in the mean time, R_0, R_2, and C_2 change from 0.0013 Ω, 0.0024 Ω, and 440.57F to 0.0008 Ω, 0.0010 Ω, and 200.00F, respectively. Thus, the above listed three groups can reflect the variation of parameters. Based on the three groups of parameters, the SOC estimation results under the HWFET drive cycle are shown in Figs. 23–25, respectively, with comparison with the Coulomb counting method.

In Fig. 23, the SOC estimated with the inaccurate parameters is higher than that with the accurate parameters all the time. It is lower than the SOC estimated based on the Coulomb counting method before 400 s and higher afterward. The maximum SOC difference between using the accurate and inaccurate parameters is within 5%. In Fig. 24, the SOC estimated with the inaccurate parameters is always lower than that with the accurate parameters, and the maximum difference is less than 3%. In Fig. 25, the results are similar to that in Fig. 23. The SOC estimated with the inaccurate parameters is higher than that with the accurate parameters. Based on the above analysis, the battery SOC varies with different parameters, and the proposed algorithm relies on the battery parameters, but the dependence on the parameter accuracy is not so great, i.e., the SOC is still within 3–5% error with parameter changing at 50%. However, to increase the SOC estimation accuracy, for each cell in the EDV system, the parameters should be identified in advance to ensure the precision of the proposed algorithm.

VI. CONCLUSION

In this paper, an SOC estimation algorithm based on EKF has been developed. A nonlinear battery model consisting of an open circuit voltage and a two-order RC circuit in series is constructed. The EKF method is applied to estimate the battery SOC with the proposed model. A hardware-in-the-loop test bench is built to simulate the vehicle and test the battery under different drive cycles. The results show that the proposed algorithm is more accurate for estimating the SOC. It does not rely on the initial SOC and is immune to parameter errors. In conclusion, the proposed algorithm can provide an accurate estimation of the SOC for an EDV battery system.

Nevertheless, the model does not consider the influence of temperature nor the aging effect, which can affect the battery SOC estimation. We plan to perform further work in this area as our next area of study.

REFERENCES

[1] A. F. Burke, "Batteries and ultracapacitors for electric, hybrid, and fuel cell vehicles," *Proc. IEEE*, vol. 95, no. 4, pp. 806–820, Apr. 2007.

[2] E. Tara, S. Shahidinejad, S. Filizadeh, and E. Bibeau, "Battery storage sizing in a retrofitted plug-in hybrid electric vehicle," *IEEE Trans. Veh. Technol.*, vol. 59, no. 6, pp. 2786–2794, Jul. 2010.

[3] V. Agarwal, K. Uthaichana, R. A. DeCarlo, and L. H. Tsoukalas, "Development and validation of a battery model useful for discharging and charging power control and lifetime estimation," *IEEE Trans. Energy Convers.*, vol. 25, no. 3, pp. 821–835, Sep. 2010.

[4] A. Szumanowski and C. Yuhua, "Battery management system based on battery nonlinear dynamics modeling," *IEEE Trans. Veh. Technol.*, vol. 57, no. 3, pp. 1425–1432, May 2008.

[5] W. Le Yi, M. P. Polis, G. G. Yin, C. Wen, F. Yuhong, and C. C. Mi, "Battery cell identification and SOC estimation using string terminal voltage measurements," *IEEE Trans. Veh. Technol.*, vol. 61, no. 7, pp. 2925–2935, Sep. 2012.

[6] U. S. Kim, C. B. Shin, and C.-S. Kim, "Modeling for the scale-up of a lithium-ion polymer battery," *J. Power Sources*, vol. 189, no. 1, pp. 841–846, Apr. 2009.

[7] G. Lijun, L. Shengyi, and R. A. Dougal, "Dynamic lithium-ion battery model for system simulation," *IEEE Trans. Compon. Packag. Technol.*, vol. 25, no. 3, pp. 495–505, Sep. 2002.

[8] Y.-S. Lee, W.-Y. Yang, and T.-Y. Kuo, "Soft computing for Battery State-of-Charge (BSOC) estimation in battery string systems," *IEEE Trans. Ind. Electron.*, vol. 55, no. 1, pp. 229–239, Jan. 2008.

[9] Y. Hu, S. Yurkovich, Y. Guezennec, and B. J. Yurkovich, "A technique for dynamic battery model identification in automotive applications using linear parameter varying structures," *Control Eng. Pract.*, vol. 17, no. 10, pp. 1190–1201, Oct. 2009.

[10] G. L. Plett, "Extended Kalman filtering for battery management systems of LiPB-based HEV battery packs: Part 3. State and parameter estimation," *J. Power Sources*, vol. 134, no. 2, pp. 277–292, Aug. 2004.

[11] G. L. Plett, "Extended Kalman filtering for battery management systems of LiPB-based HEV battery packs: Part 2. Modeling and identification," *J. Power Sources*, vol. 134, no. 2, pp. 262–276, Aug. 2004.

[12] G. L. Plett, "Extended Kalman filtering for battery management systems of LiPB-based HEV battery packs: Part 1. Background," *J. Power Sources*, vol. 134, no. 2, pp. 252–261, Aug. 2004.

[13] D. V. Do, C. Forgez, K. El Kadri Benkara, and G. Friedrich, "Impedance observer for a li-ion battery using Kalman filter," *IEEE Trans. Veh. Technol.*, vol. 58, no. 8, pp. 3930–3937, Oct. 2009.

[14] Y. Hu and S. Yurkovich, "Linear parameter varying battery model identification using subspace methods," *J. Power Sources*, vol. 196, no. 5, pp. 2913–2923, Mar. 2011.

[15] C. Min and G. A. Rincon-Mora, "Accurate electrical battery model capable of predicting runtime and I-V performance," *IEEE Trans. Energy Convers.*, vol. 21, no. 2, pp. 504–511, Jun. 2006.

[16] Y. He, W. Liu, and B. J. Koch, "Battery algorithm verification and development using hardware-in-the-loop testing," *J. Power Sources*, vol. 195, no. 9, pp. 2969–2974, May 2010.

[17] K. Il-Song, "Nonlinear state of charge estimator for hybrid electric vehicle battery," *IEEE Trans. Power Electron.*, vol. 23, no. 4, pp. 2027–2034, Jul. 2008.

[18] G. Welch and G. Bishop, An Introduction to the Kalman Filter, Univ. Carolina, Chapel Hill, NC. [Online]. Available: http://www.cs.unc.edu/~welch/kalman/kalmanIntro.html

[19] Z. Bingzhan, C. C. Mi, and Z. Mengyang, "Charge-depleting control strategies and fuel optimization of blended-mode plug-in hybrid electric vehicles," *IEEE Trans. Veh. Technol.*, vol. 60, no. 4, pp. 1516–1525, May 2011.

Zheng Chen (A'10) received the B.S.E.E. and M.S.E.E. degrees in electrical engineering and the Ph.D. degree in control science engineering from Northwestern Polytechnical University, Xi'an, China, in 2004, 2007, and 2012, respectively.

He was a Visiting Scholar with the University of Michigan-Dearborn from 2008 to 2011, where he is currently a Postdoctor with the Department of Electrical and Computer Engineering. His research interests are battery management systems, battery modeling and status estimation, and energy management of hybrid electric vehicles.

Yuhong Fu received the M.S. degree in automotive systems engineering from the University of Michigan-Dearborn in December 2011.

She is currently with General Motors, Inc., Warren, MI. Her research interests are battery modeling and management for electric drive vehicle applications.

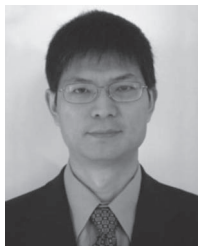

Chunting Chris Mi (S'00–A'01–M'01–SM'03–F'12) received the B.S.E.E. and M.S.E.E. degrees in electrical engineering from Northwestern Polytechnical University, Xi'an, China, and the Ph.D. degree in electrical engineering from the University of Toronto, Toronto, ON, Canada.

He was previously an electrical engineer with General Electric Canada, Inc. He is currently a Professor of electrical and computer engineering and the Director of the newly established Department of Energy-funded GATE Center for Electric Drive Transportation, University of Michigan-Dearborn. He has conducted extensive research and published more than 100 articles. His research interests include electric drives, power electronics, electric machines, renewable-energy systems, and electrical and hybrid vehicles.

Dr. Mi was the Chair (2008–2009) and Vice Chair (2006–2007) of the IEEE Southeastern Michigan Section and the General Chair of the Fifth IEEE Vehicle Power and Propulsion Conference held in Dearborn on September 6–11, 2009. He has been an Associate Editor for the IEEE TRANSACTIONS ON VEHICULAR TECHNOLOGY, the IEEE TRANSACTIONS ON POWER ELECTRONICS LETTERS, and the IEEE TRANSACTIONS ON INDUSTRY APPLICATIONS and a Senior Editor for the *IEEE Vehicular Technology Magazine*. He has been a Guest Editor for the *International Journal of Power Electronics* and Associate Editor for the *Journal of Circuits, Systems, and Computers* (2007–2009). He serves on the Editorial Board of the *International Journal of Electric and Hybrid Vehicles* and *IET Electrical Systems in Transportation*. He received the "Distinguished Teaching Award" and "Distinguished Research Award" from the University of Michigan-Dearborn, the 2007 IEEE Region 4 "Outstanding Engineer Award," the "IEEE Southeastern Michigan Section Outstanding Professional Award," and the "SAE Environmental Excellence in Transportation Award."